Radio Science, Volume 29, Number 1, Pages 293–309, January–February 1994

Coordinated convection measurements in the vicinity of auroral cavities

R. A. Doe,[1,2] M. Mendillo,[1] J. F. Vickrey,[3] J. M. Ruohoniemi,[4] and R. A. Greenwald[4]

Meridional radar scans of electron density from the Sondrestrom incoherent scatter radar (Greenland, 66.99°N, 50.95°W) have been used to identify latitudinally narrow, field-aligned depletions of the auroral F region ionosphere. Observations of these so-called "auroral cavities" have been reported in earlier case studies in close proximity to E layer arcs at the poleward edge of the nightside oval (*Doe et al.* 1993). These radar data indicated that the cavities and arcs remained as collocated pairs for periods as long as an hour, while coordinated imaging and satellite measurements indicated that the pairs were extended in magnetic local time. These observations suggested at least two causal mechanisms: (1) cavity formation by the convective distortion of an existing density depletion, or (2) cavity formation by vertical evacuation from a downward field-aligned current. New results from a model developed to examine the convection mechanism suggest that a distorted polar cap density depletion will elongate parallel to the local convection streamline when observed in the morning sector (far from the location of divergent flow lines or the Harang discontinuity). In order to establish evidence for these two mechanisms and further refine the physical properties of auroral cavities, a joint imaging/radar experiment was carried out in February 1991, at the Sondrestrom and Goose Bay (Labrador, 54.4°N, 60.4°W) radars with an emphasis on multispectral imaging, horizontal convection and off-meridional density measurements. When compared to coincident all-sky images, the convection data indicate significant cross-arc flow during cavity formation sequences on 6 and 10 February, 1991, questioning the applicability of mechanism (1). A third example on February 8, 1991, shows the alignment of a cavity/arc pair with the local streamline at the edge of an E region auroral arc. This last example illustrates the difficulty in establishing the relative dominance of either mechanism for a particular event. The continued association of cavities with auroral precipitation and failure to detect elongated cavities or those oriented along the local convection streamline lead to the conclusion that cavities are probably created by localized field-aligned currents.

[1]Center for Space Physics, Boston University, Boston, Massachusetts.

[2]Now at Geoscience and Engineering Center, SRI International, Menlo Park, California.

[3]Geoscience and Engineering Center, SRI International, Menlo Park, California.

[4]The Johns Hopkins University Applied Physics Laboratory, Laurel, Maryland.

Paper number 93RS02129.
0048-6604/94/93RS-02129$08.00

1. INTRODUCTION

Latitudinally narrow depletions of ambient polar cap F region plasma were observed at the poleward edge of the nightside auroral oval by the Sondrestrom incoherent scatter (IS) radar in January 1987 [*Doe et al.* 1989]. Such "auroral ionospheric cavities" were subsequently identified in a Sondrestrom IS radar data base of elevation scans in the magnetic meridian during three consecutive winters (1986-1988). The observed cavities had average densities 45% below adjacent polar cap values, tracked the poleward edge of E layer aurora for periods up to an hour, and formed

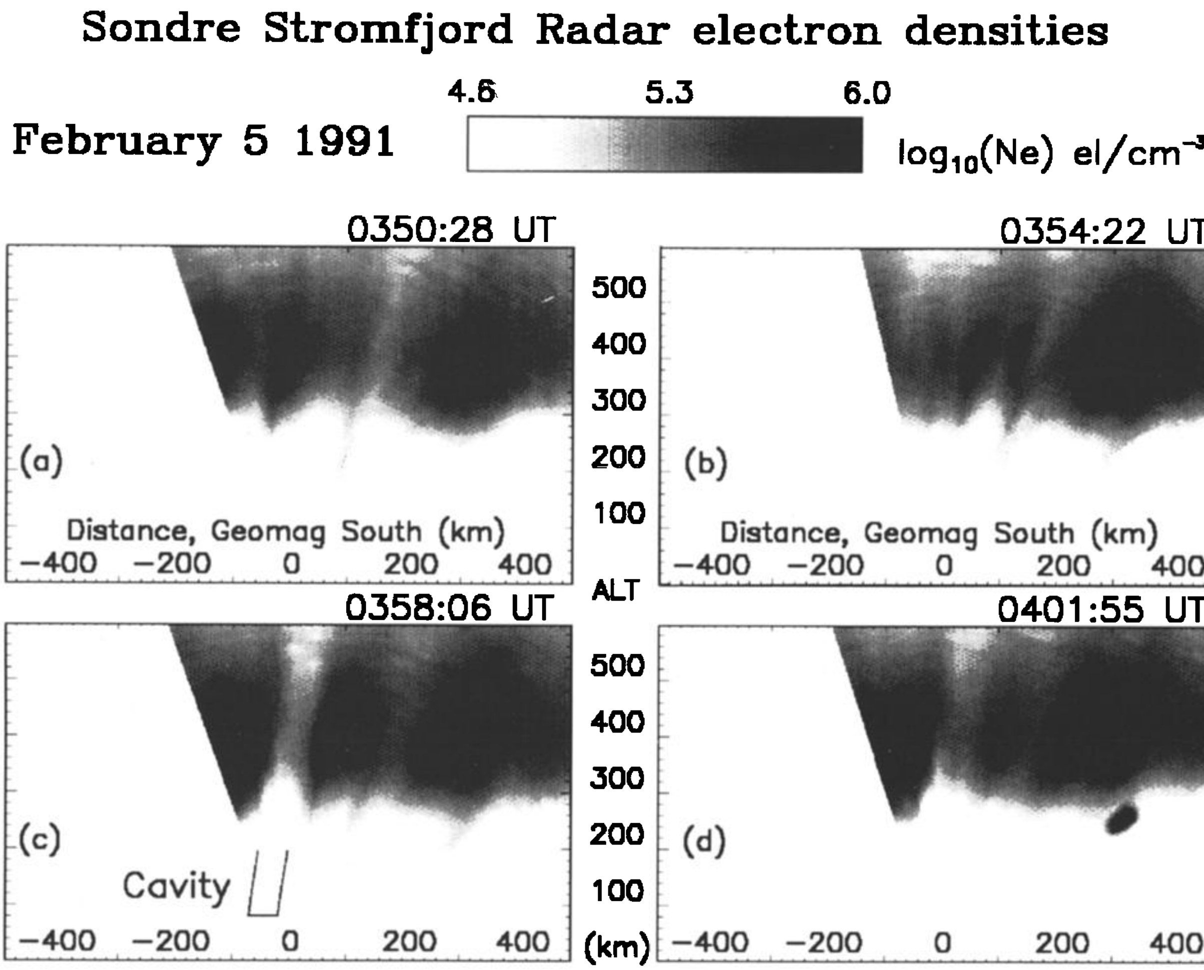

Fig. 1. An auroral cavity formation event observed with the Sondrestrom IS radar during four sequential meridional radar scans on February 5, 1991. Each scan spans 1000 km along the horizontal axis and 600 km along the vertical axis, with the log of electron density represented with a gray scale over a range from 4.6 to 6.0 electrons cm^{-3}, as indicated. The cavity is just poleward of a system of *F* region arcs at 0200 MLT in the third of panel.

on time scales as short as a few minutes [*Doe et al.* 1993]. The key feature of auroral cavities is their field-aligned morphology. Figure 1 illustrates a more recent example of cavity formation observed during solar maximum conditions in the post-midnight sector. Each panel of this figure is a vertical slice through the geomagnetic meridian with 1000 km of N-S distance along the horizontal axis and 600 km of altitude along the vertical axis. A cavity appears near zenith in Figure 1*c* with the characteristic signatures of being poleward of the auroral *E* layer ionization (N_e "finger" at ~150 km) and showing a concave bottomside N_e in the *F* region (height >200 km).

In the original study [*Doe et al.* 1993] hereafter referred to as paper 1], radar-measured plasma parameters and a model neutral atmosphere were used to examine chemical recombination and vertical diffusion as cavity formation mechanisms; these mechanisms were shown to be nonviable for the examples presented. The results in paper 1 did not provide information to distinguish between two other possible cavity formation mechanisms: convecting gradients and downward field-aligned currents (FACs).

In the convecting gradient, or "drift mechanism," an existing electron density depression in the polar cap is convectively distorted and stretched out along an $\mathbf{E} \times \mathbf{B}$ streamline during transit to the nightside oval. Although the alignment of an evolving, elongated structure need not be exclusively parallel to the local streamline, especially near regions of diverging convection streamlines, modeling results reported herein suggest that most mature (lifetime $\sim$4 hr), thin structure is stretched out along the flow direction.

Cavity creation by this method requires an initial polar cap "seed" density depression. The density depletion at the core of the seed should be sufficiently deep to allow cavity formation in a time scale over which the convection pattern remains stable. Although the precise details of seed formation need not be specified, it could result from mechanisms previously rejected in paper 1 as too slow for rapid, in-situ cavity creation. These processes included localized, enhanced chemical recombination and vertical diffusion. The scale size of the seed can span a wide range of values, although a narrow seed would, in essence, already qualify as a cavity. As a starting point, this study will focus attention on the creation of cavities from the convective distortion of density depressions on the largest scale ($\sim$600 km).

This scenario is analogous to the mechanism posed by *Robinson et al.* [1985] for the production of medium-scale ionization enhancements from the distortion of a large-scale plasma "blob." The global convection pattern affects the evolution of plasma structure in three ways: (1) it stretches the seed into an elongated shape, (2) it steepens gradients at the edge of the density depression and (3) it moves the structure into the radar field of view. A model of auroral cavity formation via this mechanism is presented in section 2 to compare with the observations of paper 1 and to illustrate the motivation for the subsequent validation experiment reported herein.

An alternative mechanism creates auroral cavities by evacuating ionospheric electrons vertically and ions horizontally in response to an arc-related system of field-aligned currents (FACs) and Pedersen currents. This "FAC mechanism" follows the theoretical suggestion of *Block and Fälthammar* [1968] and the trough observations of *Klumpar* [1979] and *Rich et al.* [1980] that thermal ionospheric electrons are evacuated upward as the charge carriers of a downward Birkeland current. Such field-aligned evacuation is circumstantially supported by the close association of cavities with E layer arcs and a satellite measurement of downward/upward field-aligned currents directly above a cavity/arc pair [*Doe et al.* 1993].

This paper describes a joint radar/optical experiment at the Sondrestrom IS radar facility designed to characterize the horizontal morphology and convection environment of auroral cavities in an attempt to differentiate between the two formation mechanisms. Specifically, the horizontal morphology of cavities and convective flow in the near vicinity were examined for evidence to support the convective distortion mechanism. The first experimental goal, therefore, was to measure the convection velocities around the cavity for comparison with cavity orientation, and the second experimental goal was to measure the typical azimuthal extent of cavities after they were detected over the radar. The IS radar was operated for approximately 40 hours during seven consecutive nights during the dark moon period of February 3-10, 1991. This experiment augments the earlier meridional scan method with off-meridional scans, local azimuth scans of ion velocity, and coordinated HF radar velocity measurements from Goose Bay, Labrador. The observations spanned a period when the IMP 8 satellite was in the solar wind, enabling a comparison of cavity data with a convection model parameterized by the interplanetary magnetic field (IMF) orientation. During meridional radar scans, overhead convection estimates were made by combining E region Pedersen drifts with a suitable mobility model. Thus three methods were used to infer the convection pattern: local Sondrestrom IS radar estimates, merged Goose Bay/Sondrestrom radar azimuth scans, and a *Heppner and Maynard* [1987] empirical model.

Direct imaging of auroral cavities is complicated by the small difference between cavity and polar cap airglow intensity, approximately 20 R, and their close proximity to bright ($\sim$2 kR) auroral arcs. Thus an all-sky optical imager was used to establish the auroral arc context for radar cavity observations. Section 3 describes the experimental plan and provides a brief summary of the February 1991, campaign. The subsequent sections describe two morning sector cavity events that lend support to the FAC mechanism. A final case study period shows a cavity adjacent to an auroral arc which is aligned with a large-scale zonal flow channel. This cavity event may be under the influence of both FAC and drift formation mechanisms.

2. MODELED DRIFTING GRADIENTS

The *Robinson et al.* [1985] model for the production of medium-scale F region structure shows that a nightside "tongue" of L shell-aligned ionization can form from a circular ionization enhancement after 4 hours of steady state convection. If the initial density structure is assumed to be a density depression, rather than an enhancement, then the final feature will be observed in the magnetic meridian as a narrow density depression, or cavity. *Heelis* [1992], in a steady state model of polar cap "patch" formation, points out that ionization gradients perpendicular to the plasma flow are easily formed by the action of convection alone. The model described herein is used to qualitatively determine the possible source regions for cavities created by the drift mechanism. The model additionally seeks to determine the time scale required to create the relatively deep depletions observed in cavities from large-scale plasma depressions with relatively shallow cores. The classic "polar hole" will serve as a model for such seed structure as it is the largest density depletion observed in the polar cap and has a well documented density profile.

While it might seem intuitive to assume that a distorted plasma gradient will stretch out along **E** × **B** convection streamlines, modeling suggests that intermediate-scale features, which are larger than the latitudinal width of cavities, will form at significant angles with respect to the flow. Seed density structure on convection streamlines that diverge, as in the case of the those that connect to the Harang discontinuity, will also form elongated structures that are not parallel to the local flow. In such cases, the seed will stretch as it crosses the discontinuity as one part tries to convect westward and another part tries to convect eastward. Nevertheless, seed structure on paths that thread through regions of converging equipotentials, such as the convection "throat" region, or on paths that approach stagnation points will form elongated structure parallel to local streamlines.

The distorted blobs shown in the third and fourth panels in Figure 8 of the *Robinson et al.* [1985] study are an excellent example of seed structure on divergent flow lines. These distorted shapes form from a blob that is placed in the polar cap on streamlines that diverge at the location of the Harang discontinuity. The resultant shapes are streamline-aligned only near the core of the duskside cell and are orthogonal to the flow at the midpoint of the Harang discontinuity.

In order to further illuminate the dependence of these final shapes on the initial seed location, a convective distortion model has been designed. This model tracks the evolution of a plasma seed in a user-specified empirical convection pattern. For the following model runs, the seed was chosen to be a 6° diameter circular depletion with a core density 85% below that of the surrounding F region. These values have been selected to be consistent with AE-C satellite polar hole-type characteristics reported by *Brinton et al.* [1978]. It should be emphasized that this choice is for illustration purposes, using a naturally occurring depression, and does not imply that cavities result from the classic polar hole. The *Heppner and Maynard* [1987] convection model was chosen for the first several runs. This convection model is parameterized by IMF orientation and K_p index, thereby allowing convenient comparison with observational data.

Distorted plasma seeds are shown in Figures 2*a* and 2*b* for two convection patterns appropriate for IMF B_z south (B_y positive) and B_z north (B_y positive) conditions, respectively. These polar plots show the final shape of eight initially circular seeds, placed at uniformly spaced magnetic local time (MLT) positions within the pattern, after 4 hours of convective dis-

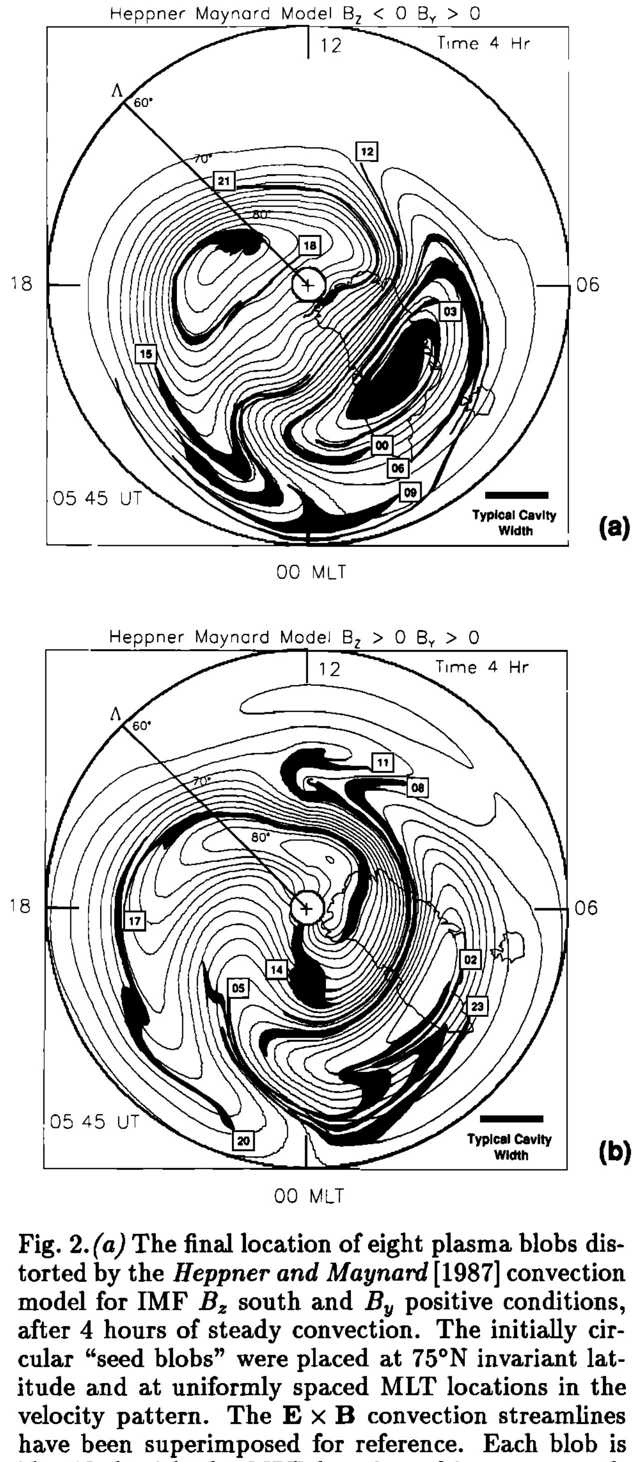

Fig. 2. *(a)* The final location of eight plasma blobs distorted by the *Heppner and Maynard* [1987] convection model for IMF B_z south and B_y positive conditions, after 4 hours of steady convection. The initially circular "seed blobs" were placed at 75°N invariant latitude and at uniformly spaced MLT locations in the velocity pattern. The **E** × **B** convection streamlines have been superimposed for reference. Each blob is identified with the MLT location of its corresponding seed. With the exception of the "09" blob, most thin structures are aligned with convection streamlines. *(b)* The results of an analysis similar to Figure 2*b* for IMF B_z north and B_y positive conditions.

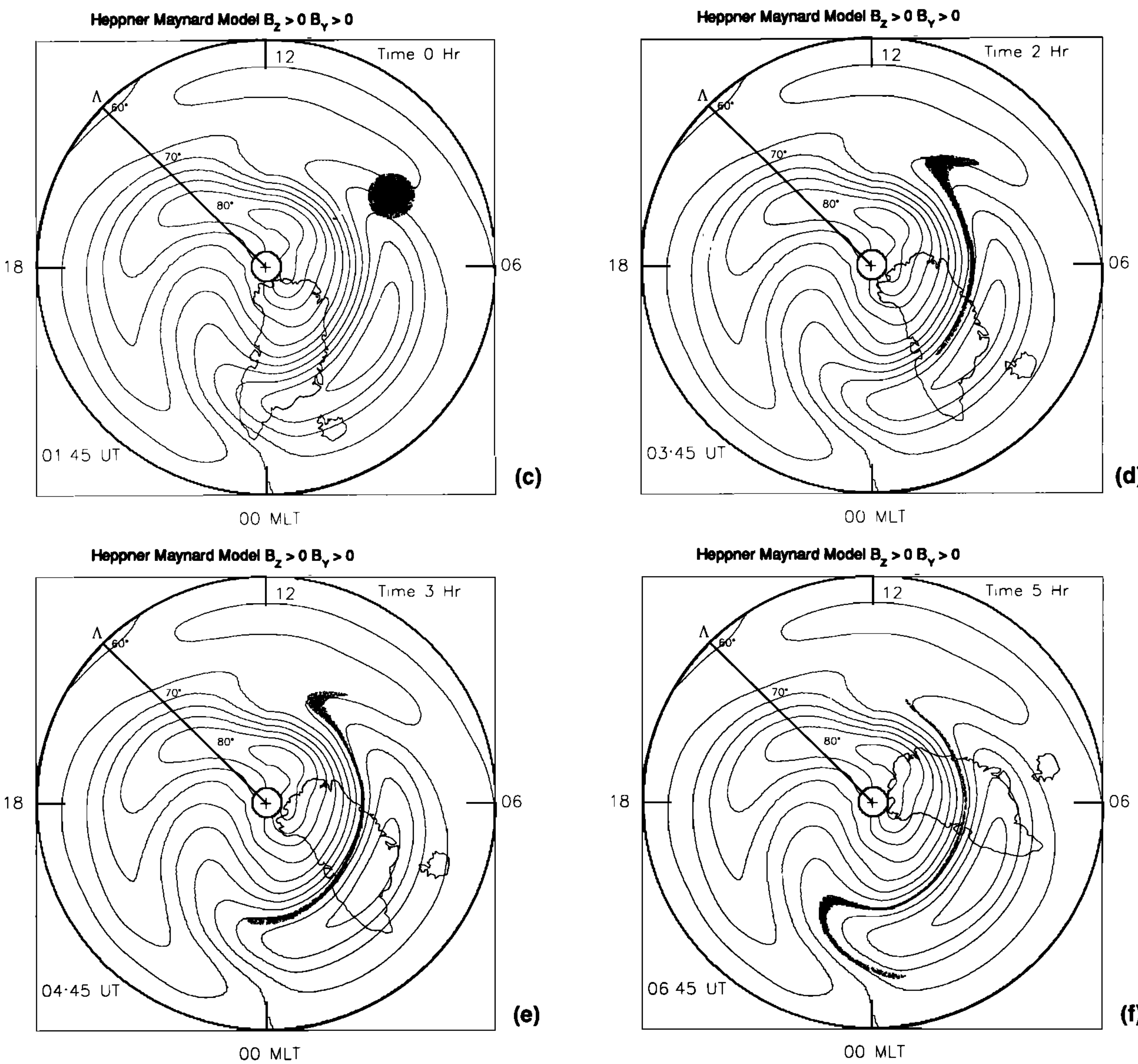

Fig. 2.(continued) Four sequential polar views of a large-scale plasma depletion, or polar hole, placed in an convection pattern chosen for the IMF B_z north and B_y positive conditions measured by the IMP 8 satellite on February 6, 1991. *(c)* Initial plasma depletion at 72° invariant latitude and 0800 MLT. *(d)* Two hours of drift with polar hole stretched into a thin tongue of depleted plasma over the east coast of Greenland. *(e)* Plasma structure, above Sondrestrom, 3 hours later with latitudinal density gradient 4 times larger than the initial polar hole density gradient. *(f)* Plasma structure at the edge of the Sondrestrom radar's field of view after an additional 2 hours of convection.

tortion. A 4 hour period was determined to be the characteristic time required to create narrow structure on the scale of the average latitudinal width of cavities. The seed depressions were all located at 75° invariant latitude, and the final shapes are labeled with the MLT location for the position of their respective seeds. The shapes labeled "09" in Figure 2*a* and "20" in Figure 2*b* have been distorted while passing through the Harang discontinuity and display thin cavity-like structure that is not aligned with the local flow orientation. These shapes best correspond to the example shown in the *Robinson et al.* [1985] study. Nonaligned medium-scale structure can additionally be observed for shapes labeled "18" and "03" in Figure 2*a*. For the remaining cases, however, narrow features are aligned along convection streamlines. The modeling result that cavity-scale distortions preferentially align along the local $\mathbf{E} \times \mathbf{B}$ streamline, away from regions with significant flow divergence, has been additionally verified using the convection models of *Heelis et al.* [1982] and *Holt et al.* [1987].

Figures 2*c* through 2*f* show the evolution of a circular seed in the *Heppner and Maynard* [1987] convection pattern specified for the IMF B_z north and B_y positive conditions measured on February 6, 1991, during an auroral cavity observation campaign (Plate 2, discussed in section 4.2). The initial and evolved plasma shapes have been shaded to show their relative cross-sectional densities. Because of the wide range of F region densities measured during cavity events, the initial and final density depletions are quantified in units of relative percent depletion (below polar cap F region average density) per half width at half minimum in kilometers. Thus the initial 6° polar cap density depletion described previously has a density gradient of -0.30% km^{-1} from edge to center. If chemical decay significantly erodes this relative depletion, which it can on a time scale of several hours, then the convection field must additionally compress the gradient in order to create a cavity-like density signature. Nominal estimates of recombination time from paper 1 indicate that decay can decrease this initial density gradient by 10% to a value of -0.27% km^{-1} from edge to center, in 1 hour.

The seed has been initially located in the morning sector at 72° invariant latitude and 0800 MLT. Within 3 hours, the seed has been stretched out along a streamline that crosses Sondrestrom's zenith. At this point, the structure has a meridional density gradient of -1.24% km^{-1} which compares favorably with the -1.31% km^{-1} average cavity density gradient calculated from Table 1 of paper 1 and the observed gradient of -1.67% km^{-1}, measured at 0437:45 UT on February 6, 1991 (Plate 2*c*). This cavity remains within the Sondrestrom radar's field of view for an additional hour.

Multiple runs of this model indicate that thin cavity structure will form over the Sondrestrom radar as long as the initial density depression is placed within 2 hours MLT of the convection throat region (70° latitude and 1000 MLT). This result is reasonable since the growth rate for gradients on scale of a cavity is directly proportional to the velocity parallel to the initial gradient, provided velocity structure exists on the same scale size. Kelley [1989] quantifies this relationship in a description of the anisotropic evolution of drifting F region structure in a convection electric field that has spatial structure orthogonal to the initial plasma gradient. This relationship can be cast in terms of the convection velocity,

$$\gamma(k) = \frac{v_{\|}(k)}{L}, \tag{1}$$

where γ is growth rate, $v_{\|}(k)$ is the velocity parallel to the initial gradient, and L is the initial gradient scale length. The convection throat region is characterized by both enhanced velocities and velocity gradients at the same scale size as a cavity. Equation (1) implies that increasing the velocity at the polar hole boundary can increase the growth rate of cavity scale structure. Indeed, the 3-hour time scale required to form a cavity in the quiet time (IMF B_z north) convection pattern of Figure 2 can be reduced to 90 min in a moderately disturbed (K_p = 3) IMF B_z south pattern.

To summarize, this model suggests that cavities should be elongated and relatively long-lived. The model predicts that these features should be oriented with the local streamline, provided measurements are made far from regions of significant flow divergence. Thus only morning sector events located poleward of 72°N invariant latitude (presumably far from the Harang discontinuity) are reported herein.

3. EXPERIMENTAL PLAN

3.1. *Cavity detection*

The February 1991, period was chosen, on the basis of the results in paper 1, to maximize the statistical likelihood for cavity observation and opportunities for all-sky imaging. Initial cavity detections were made by sampling the magnetic meridian with 5-min, 120° elevation scans in an alternating S-N and N-S "windshield wiper" mode. The angular and range resolution of these scans were designed to yield approximately "square" samples at 300 km. Once a cavity was detected, the elevation range was reduced to 90° (centered on the cavity), in order to maximize time resolution. Monochromatic all-sky images at 6300-Å and 4278-Å were gathered throughout the event to establish the orientation of arcs near the cavity.

The previous study invoked selection criteria for cavity observations that yielded 29 events from a 2-year data base of radar scans. The selection rules rejected scans with significant polar cap F region structure (e.g., patches and Sun-aligned arcs) in order to make precise measurements of evacuation fluxes. This requirement and the requirement that cavities be observed adjacent to auroral E region ionization were relaxed for the February 1991, campaign. Although low-altitude E region arcs were typically observed

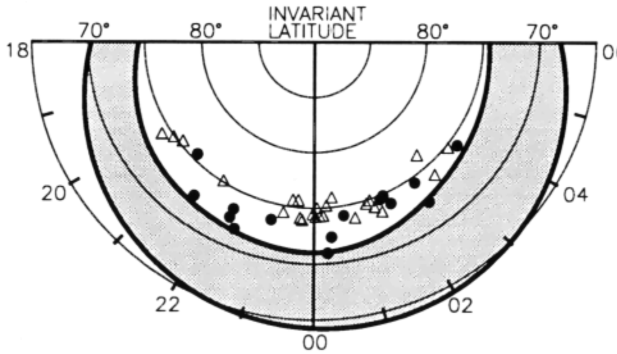

Fig. 3. Total cavity observations for the previous and current cavity studies on a nightside polar grid of MLT versus invariant latitude. Triangles indicate observations from the 2-year *Doe et al.* [1993] study; circles indicate cavities observed from February 3 to February 10, 1991. The grid includes the *Feldstein and Starkov* [1967] quiet time auroral oval for reference.

near cavities, two examples were observed adjacent to higher-altitude F region arcs (at ~170 km) far from the oval (see Figure 1 and Plate 2) and cases near patches (Plate 1). In total, 14 cavity events were observed. A summary plot of all cavity observations to date is shown on a polar MLT versus invariant latitude plot in Figure 3.

3.2. *Convection measurements*

This experiment was coordinated with the operation of the coherent-scatter HF radar located in Goose Bay, Labrador (53.4°N, 60.4°W), to better determine the drift pattern in the vicinity of cavity observations. Earlier coordinated experiments [*Ruohoniemi et al.*, 1987, 1989] have verified the Goose Bay radar's ability to measure the convective drift in a large volume common with the Sondrestrom radar, provided sufficient numbers of decameter-scale irregularities are embedded in the flow. Thus the HF radar can, in principle, provide horizontal line-of-sight convection measurements during periods when the IS radar was restricted to elevation scans. In practice, however, only two cavity formation events occurred during periods of large HF backscatter. For one period on February 8, 1991, the Sondrestrom IS radar performed a 120° azimuth scan over the HF radar backscatter volume. This second line-of-sight measurement helped further define the convection pattern by combining corresponding vector components from both radar data sets.

Whenever sufficiently dense E and F region plasma were within the IS radar's meridional field of view, estimates of the overhead convection vector were also made. The IS radar directly measures the F region meridional component, while the zonal component is inferred from the expected rotation of the E region ion velocity away from the $\mathbf{E} \times \mathbf{B}$ direction due to significant Pedersen mobility (see *de la Beaujardiere et al.* [1977] and *Heelis and Vickrey* [1990]). Despite occasional large uncertainties in zonal flow, this method provided the majority of convection measurements reported in this work.

4. CONVECTION CASE STUDIES

4.1. *Cavity formation with cross-arc flow at the auroral oval*

Plate 1 is a montage of coincident radar and imaging data gathered during a cavity formation event on February 10, 1991. The four rectangular panels show sequential radar scans in the meridian, off-meridian to the west, off-meridian to the east, and back to the meridian, respectively. The west and east scans were performed to support a coincident investigation of arc electrodynamics [*Gallagher et al.* 1993]. The first panel (1*a*) shows a relatively unstructured polar cap F region immediately adjacent to an auroral arc. Ten minutes later, during the subsequent meridional scan at 0352:37 UT, a narrow (0.4° latitude) cavity can be seen (Plate 1*g*). Depleted plasma structure in the intervening west and east scans show remarkable similarity. Although it seems that these side scans show depletion structure located on field lines directly above auroral arcs, reminiscent of dusk sector arc observations by *Weber et al.* [1991], such structure cannot be described as coaligned without a precise mapping of magnetic field lines into this off-meridional plane. If one considers the arc and polar cap plasma to be azimuthally symmetric, then these side scans seem to display a longitudinal extension of the cavity at radar zenith. The subsequent meridional scan at 0404:03 UT shows no evidence for the cavity, implying a lifetime of less than 11 min.

Six all-sky 6300-Å images which bracket this formation event are shown below the radar panels. Each image has been photometrically corrected, limited to 75° zenith distance, masked to obscure the adjacent radar dish and nearby mountain, projected to an emission height of 200 km and displayed on a Polar Anglo-American Conjugate Experiment (PACE) model geomagnetic grid. The 200-km assumed emission height is based on satellite tomographic inversion and modeling studies by *Soloman et al.* [1988]. Some residual scattered light from the adjacent mountain and van Rhijn brightening has "filled in" the weak polar cap 6300-Å emission (at low elevation angles), giving the false impression of an optical cavity signature at zenith. Such an apparent optical cavity is several degrees of latitude wide and with an emission

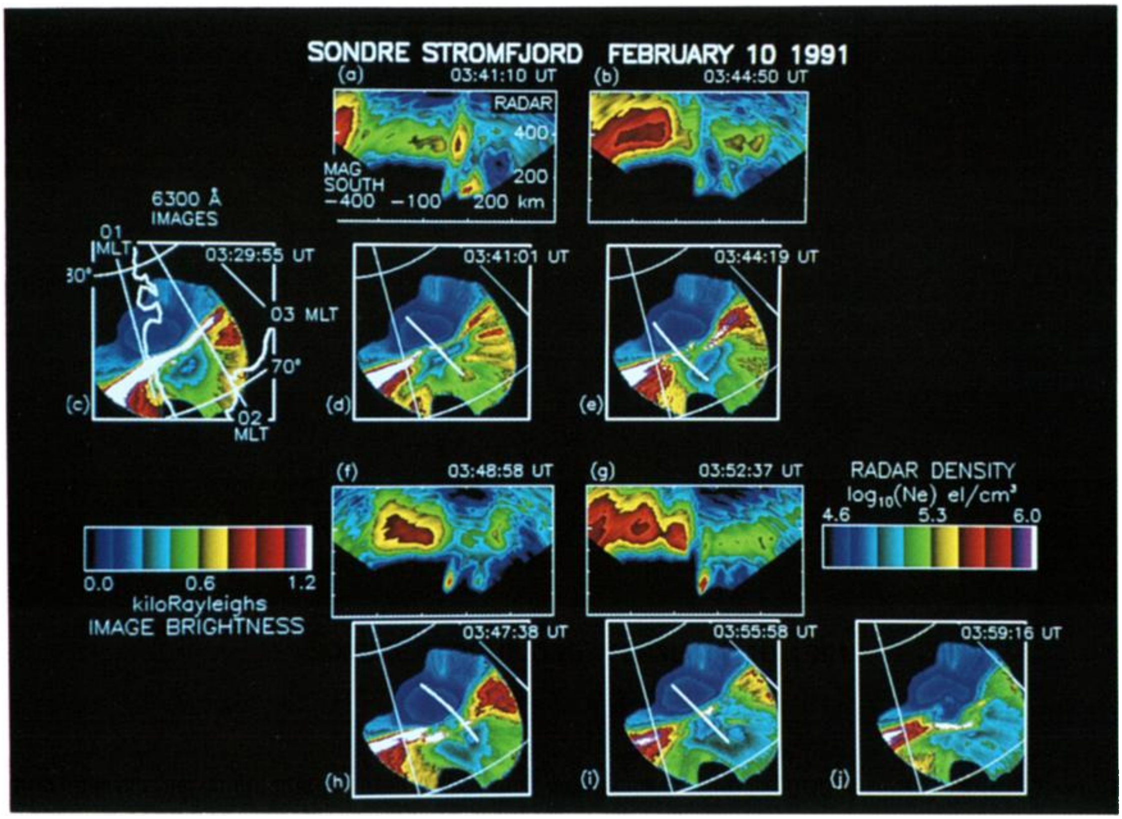

Plate 1. Sequential radar electron density scans and coordinated 6300-Å images recorded during a 10-min cavity formation event at the poleward edge of bright, relatively stationary auroral emission on February 10, 1991. Radar scans in Plates 1*(a)* and 1*(g)* are measured in the magnetic meridian, Plates 1*(b)* and 1*(f)* are measured to the west, and to the east of the meridian, respectively. The log of electron density for all scans is color-coded as in Figure 1, while white lines in Plates 1*(d)*, 1*(e)*, 1*(h)*, and 1*(i)* display the intersection of the radar scans with corresponding 6300-Å images. All radar UT times are listed at the midpoint of the 3-min 20-s scans. The six 6300-Å images have been photometrically corrected and projected onto fixed (nonrotating) geomagnetic coordinate grids with an assumed 200-km emission height. The cavity forms in the approximately 10-min period between Plates 1*(a)* and 1*(g)*.

contrast ratio of 0.5:1 (compared to polar cap airglow). Chemical airglow modeling for the observed density depletion, however, predicts a contrast ratio of only 0.1:1 across less than a degree of latitude.

The radar scan intersections at 200 km have been superimposed on coincident images. Note that the arc formation region remained bright and overhead during this event. The cavity thus formed poleward of an L shell-aligned precipitation (upward current) region.

Because the Goose Bay HF radar recorded only sporadic line-of-sight velocities during this period, the overhead velocity estimates are used for comparison. Figure 4 shows two 6300-Å images, corresponding to the times of the meridional radar scans, which have been superimposed with the estimated horizontal drift measurements. The velocity estimates gave a particularly coherent pattern as dense E and F region plasma remained near the radar zenith. The drift estimates indicate ~300 m s^{-1} equatorward flow from the north during the time of cavity formation, with the suggestion of a small zonal shear at 0355:58 UT. Since these meridional estimates are not sensitive to horizontal velocities at radar zenith, the east and west scans should be examined for evidence of cross-arc flow. Figure 5 shows the line-of-sight velocities below the density plots for the west and east side scans. Both scans show a strong velocity shear

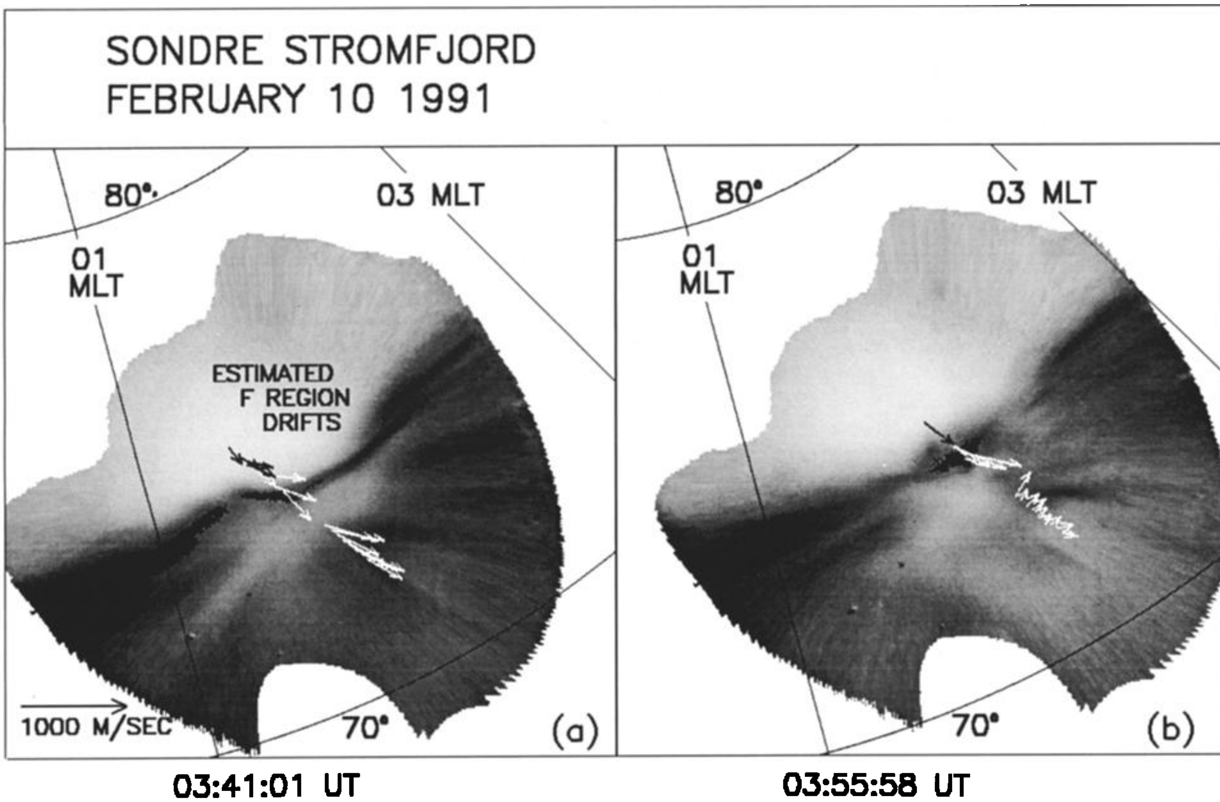

Fig. 4. Two consecutive 6300-Å images corresponding to Plates 1*d* and 1*i* with superimposed *F* region drift showing a ~300 m s^{-1} cross-arc flow during cavity formation.

associated with the arc. Moreover, all scans confirm that a large-scale flow equatorward (i.e., across the arc) exists. The equatorward motion of *F* region patches, as recorded with 1-min resolution on the Phillips Lab All-Sky Imaging Photometer (ASIP), additionally support the conclusion of significant cross-arc flow (E. Weber, personal communication, 1993).

To summarize, this short-lived cavity forms at the edge of an *L* shell-aligned arc during a period of significant cross-arc $\mathbf{E} \times \mathbf{B}$ flow. It is clearly related to precipitation signatures at its southern edge and thus is not merely the space between polar cap patches that are drifting equatorward. If the cavity is assumed to be elongated along the arc, as suggested in Plate 1, this orientation indicates a cavity that is not aligned with the streamlines of flow. Therefore this event seems to contradict the drift mechanism of cavity formation. The significant plasma flow orthogonal to the cavity and the spatial association between the cavity and the discrete arc, indicates that the FAC mechanism is a more likely explanation for the observations.

4.2. *Cavity formation with cross-arc flow in the polar cap*

Plate 2 illustrates a morning sector cavity event on February 6, 1991, with 30 min of coordinated meridional radar and 6300-Å imaging data. This period differs significantly from most other cavity observations by the absence of the auroral oval, the lack of dense *E* region plasma, and a relatively unstructured and dense (N_e ~ 5.0×10^5 el cm^{-3}) polar cap *F* region. The radar scans and 6300-Å images show that a field-aligned "finger" of bottomside *F* region ionization and associated arc remain relatively fixed in the geomagnetic frame for 30 min. *E* region arc-related emission at 4278-Å was not observed. A narrow (0.3°) field-aligned density depression is visible just north of the arc. *F* region densities in this small cavity are approximately 25% below those measured in the adjacent polar cap.

IMP 8 magnetometer data indicate that IMF B_z was north, and IMF B_y was primarily positive for an hour prior to these cavity observations. Through-

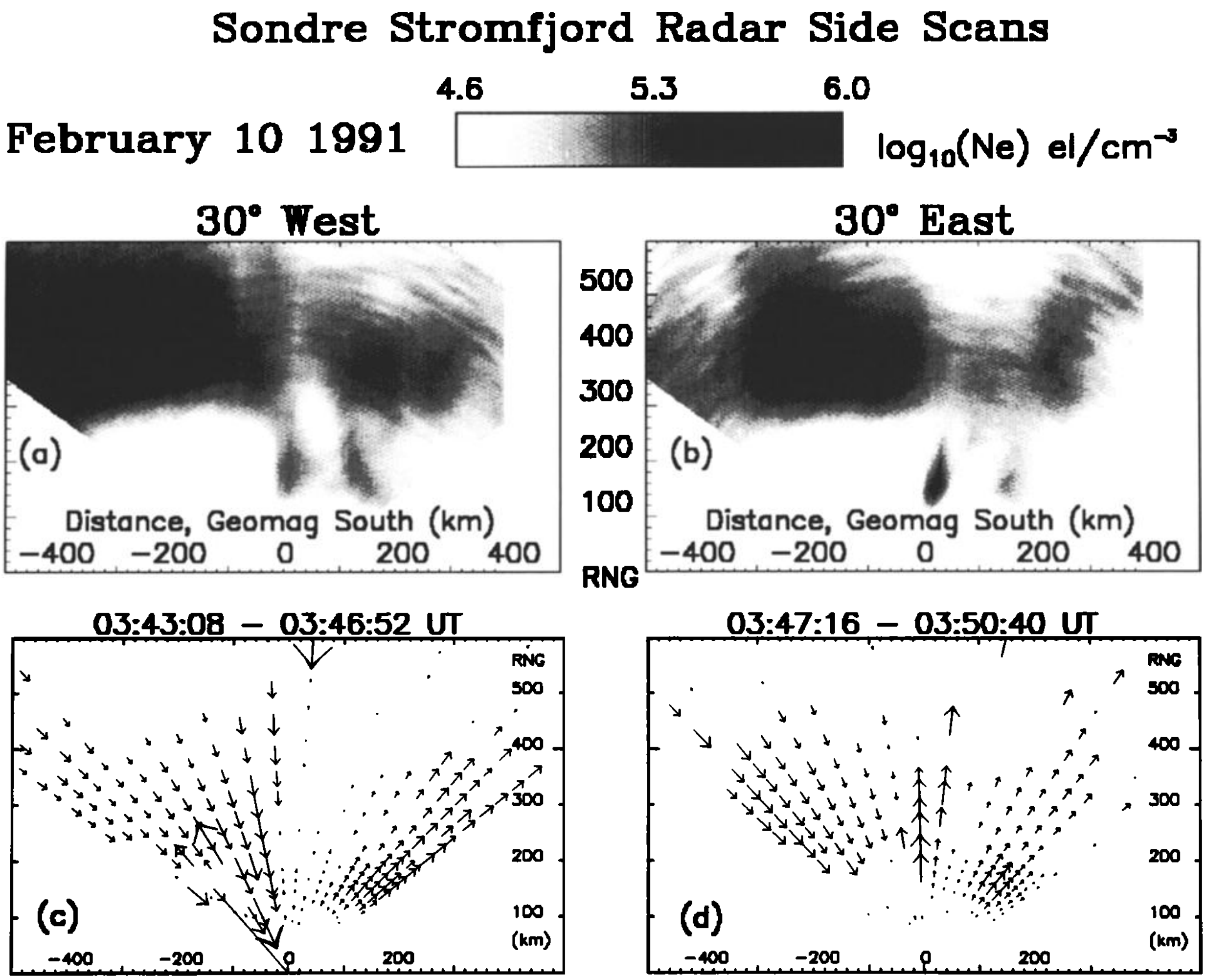

Fig. 5. *(a)* and *(b)* Two consecutive off-meridional electron density scans, corresponding to Plates 1*b* and 1*f*, with associated line-of-sight ion velocities. *(c)* Line-of-sight velocities to the west confirm the observation of a general cross-arc flow (as shown in Figure 4). *(d)* The east scan showing evidence for an eastward shear in addition to cross-arc flow.

out this period the Goose Bay HF radar measured strong backscatter. The convection velocities were primarily westward at 0400 UT with a subsequent rotation to east by 0500 UT. At 0438 UT the Goose Bay radar measured an approximately 400 m s^{-1} equatorward velocity surge coincident with the first appearance of the cavity (see Plate 2*c*). These Goose Bay velocity measurements have been analyzed by the divergence-free method described by *Ruohoniemi et al.* [1987] and superimposed, along with available Sondrestrom line-of-sight measurements and the IMF-appropriate *Heppner and Maynard* [1987] convection pattern, on the coincident 6300-Å image in Figure 6. Although the empirical convection model suggests that the arc/cavity pair is located parallel to a flow streamline, and Goose Bay measurements support the notion of drift around the southwestern tip of the modeled convection cell, both Goose Bay and Sondrestrom measurements show a significant cross-arc drift component near the location of cavity detection. The orientation of this cavity, as with the event described in Figure 4, appears to be defined by the precipitation source region, rather than by the large-scale convective flow pattern.

4.3. Streamline cavity alignment at the auroral oval

Plate 3 summarizes a cavity event with eight sequential radar scans, associated meridional drift estimates and a single 6300-Å all-sky image. Al-

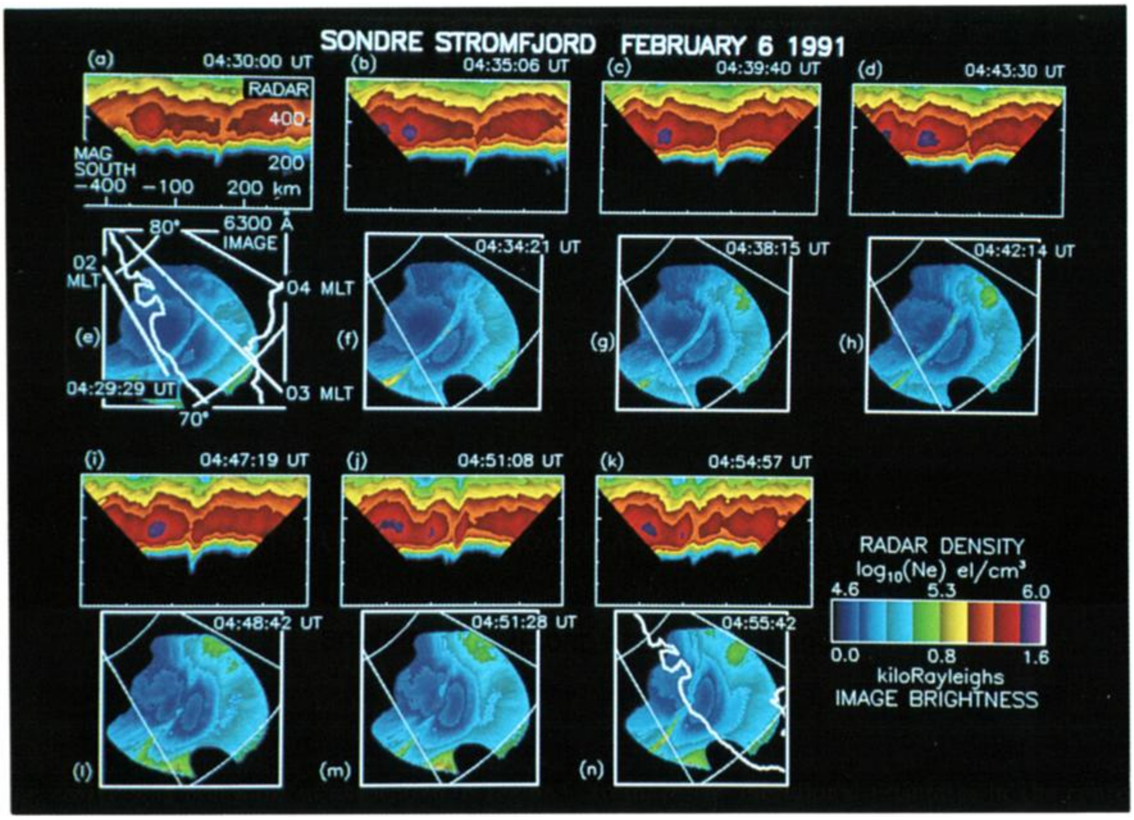

Plate 2. Meridional radar scans and 6300-Å images covering the formation of a shallow cavity on February 6, 1991. Radar scans and images are displayed as in Plate 1. *(c)* The first appearance of a small cavity just poleward of a narrow F region "finger" of ionization. This -25% relative depletion can be observed in the two following scans, *(d)* and *(i)*.

though cloud-free all-sky images were not available until 0541:33 UT (Plate 3*p*), diffuse 6300-Å auroral structure, observed through thin clouds, remained within approximately 30° of radar zenith for 40 min beforehand. This period is characterized by large F region densities poleward of a region containing E region auroral arcs. Plates 3*b*, 3*d*, 3*i*, and 3*j* clearly indicate auroral cavity structure poleward of corresponding E layer arcs on nearly identical field lines. Figure 7*a* emphasizes the persistence of these cavities with an average of the eight electron density scans made during a 30 min period when cavity signatures remained remarkably stationary. This average shows that the cavity was poleward of associated E region plasma structure and was field-aligned with a concave bottomside N_e contour. Figure 7*b* shows horizontal samples through this average scan which have been shifted to emphasize the field-aligned nature of this cavity. The sample at 300 km represents a relative density depression of approximately 30% over 0.2° of latitude.

The E and F region line-of-sight drifts and densities were of sufficient quality during this period to yield two component, horizontal vector velocity estimates. These estimates, shown in a horizontal projection below each corresponding density scan in Plate 3, suggest a strong zonal flow from west to east with some arc-related shear. The 6300-Å image at 0541:33 UT, overlayed with meridional velocity estimates in the last panel of Plate 3, clearly shows that an overhead arc is oriented parallel to the flow.

Available Goose Bay HF radar velocities, measured simultaneously with velocities from a 120° Sondrestrom azimuth scan (0509 to 0514 UT), were used to place the meridional estimates in the context of a larger flow pattern. Both velocity data sets were processed as described by *Ruohoniemi et al.* [1989], and Figure 8 shows the total merged convection pattern. The previously noted strong zonal drift appears to be part of a large-scale west to east flow pattern that extends over nearly 3 hours of local time. Thus this period reveals cavities with evidence for both FAC and

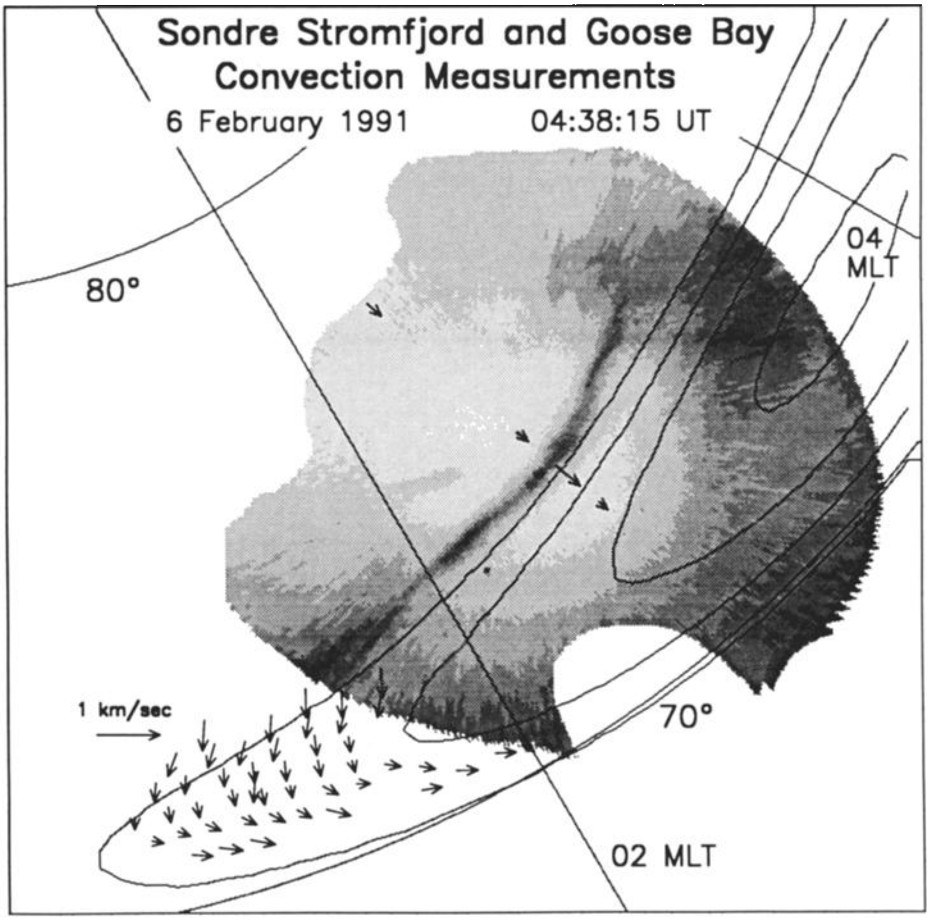

Fig. 6. Coordinated velocity measurements recorded at the time of initial cavity appearance (Plate 2*c*) superimposed on the corresponding 6300-Å image (Plate 2*g*). Streamlines from an appropriate *Heppner and Maynard* [1987] B_z north convection model are included for reference. Goose Bay measurements, grouped at the lower left of this figure, were made during a period of enhanced equatorward flow and have been rendered as true vectors with the divergence-free analysis described by *Ruohoniemi et al.* [1987]. The Sondrestrom measurements show the line-of-sight ion drift poleward of the cavity/arc pair. Both data sets support the assumption of cross-arc flow during this period.

drift formation mechanisms: close association with E region auroral arcs and orientation along the large-scale convection streamline.

5. DISCUSSION

The secondary goal of this experiment was to measure the the typical azimuthal extent of cavities. If density depletions observed in the off-meridional scans shown in Plate 1*b* and 1*f* are related to the cavity measured in the overhead scan of Plate 1*g*, then the cavity had an azimuthal width 16 min of MLT (120 km). A further refinement of this observational mode can be made by scanning along look angles chosen to intersect surfaces of constant magnetic local time at F region altitudes, to the east and west of the radar. This mode, with look angles determined from the PACE geomagnetic coordinate system [*Baker and Wing* 1989], allows the comparison of F region density features over 1 hour of MLT (15° of magnetic longitude). This method was used on five occasions during this experiment with no conclusive measurement of extended cavities.

The inability to detect elongated cavities suggests that cavities are not extended in longitude, regardless of the details of their formation. For the drift mechanism, the azimuthal extent of cavities may be small, as is the case for polar cap patches. In this

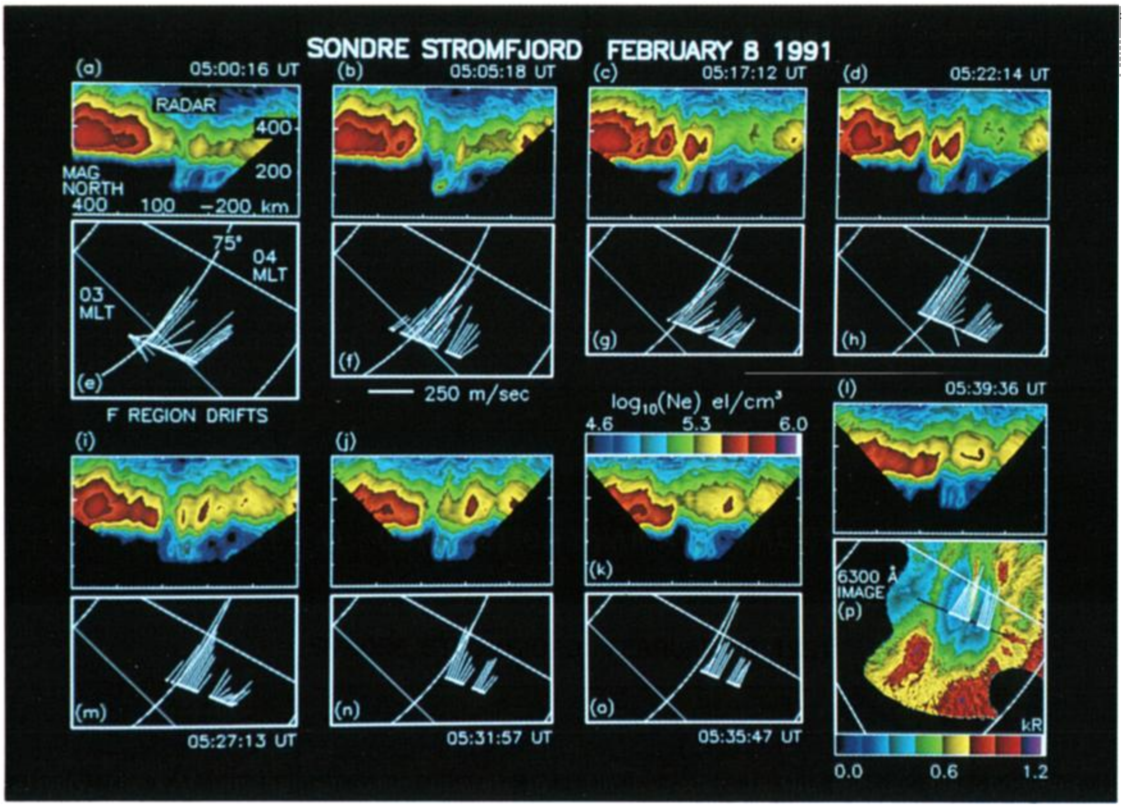

Plate 3. A series of meridional radar scans and estimated F region drifts for February 8, 1991. Radar scans for Plates 3*(a)*-3*(d)* and 3*(i)*-3*(l)* follow the same spatial and density scales described in Plate 1. Below each radar scan is a horizontal view of the overhead velocity vectors estimated from coincident E and F region drifts (see section 3.3). As can be seen from Plate 3*(p)*, because of cloudy conditions, only one 6300-Å image was available, during the radar scan at 0539 UT. Auroral cavity structure is indicated in Plates 3*(b)*, 3*(d)* and 3*(j)*, for other times it is obscured by drifting enhancements. The estimated F region drifts suggest a strong eastward zonal component throughout this period. Unlike prior observations in this study, the 6300-Å arc observed at 0539 UT is oriented parallel to the bulk flow direction.

scenario, an initial polar density depression would be stretched and, additionally, dynamically "chopped" in transit to the nightside. In their model of winter polar cap patches, *Anderson et al.* [1988] demonstrate that a burst of enhanced convection can provide the necessary density modulation. The apparent lack of elongated cavities observed throughout this experiment, however, seems to invalidate the drift process. Alternatively, the FAC mechanism could operate in confined current filaments, rather than uniform sheet currents, and produce cavities with limited azimuthal extent.

The February 1991, campaign confirmed the observation of cavities adjacent to arcs. The cavities observed here, unlike those described in paper 1, were not all located at the poleward edge of the most poleward arc (Plate 3*p*) and were not exclusively associated with E region structure (Plate 2). Even if cavities are localized in azimuth, the auroral arcs and associated optical emissions should provide a guide to the orientation of the cavity. The possibility exists, however, that this association is merely coincidental, especially for transient cavities. The short-lived cavity of February 10, 1991, for example, may simply have been drifting across the arc when scanned by the IS radar. In this specific case, however, the prior off-meridional side scans show no evidence, well poleward of the arc, for a "precursor" cavity. Therefore this cavity must have formed locally with the assumed downward "evacuation" current at the poleward edge of an L shell-aligned sheet of upward current.

The February 10, 1991, period displayed evidence of an arc-related shear superimposed on the general equatorward convection drift. This is essentially the

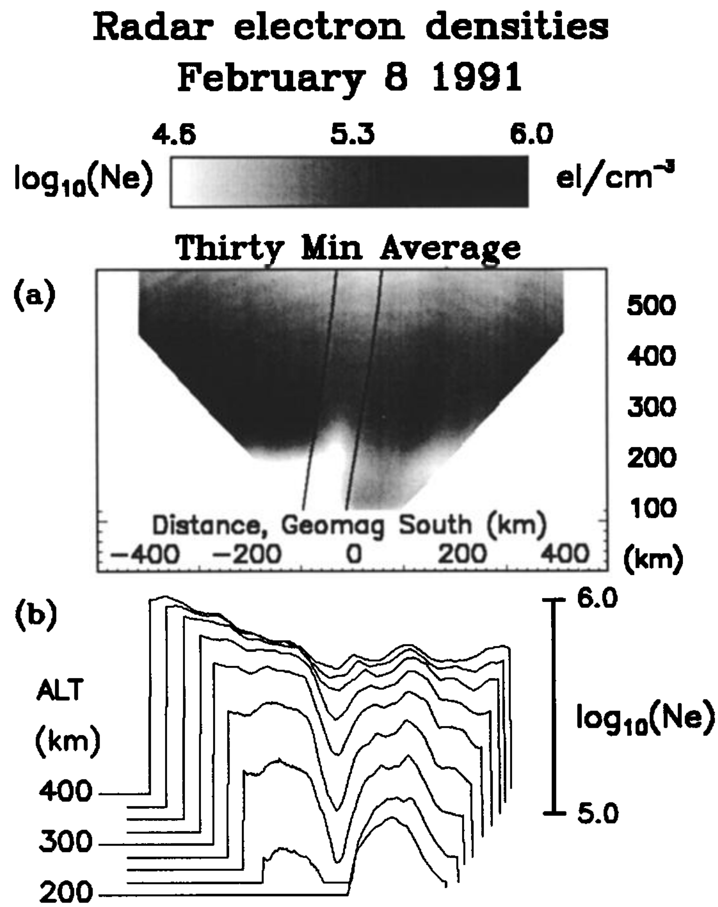

Fig. 7. (*a*) A 30-min average of radar scans which correspond to Plates 3(*a*)-3(*d*) and 3(*i*)-3(*l*). Individual radar scans have been horizontally shifted so that the location of the most poleward *E* layer arc was fixed at a common latitude. This average shows that the cavity structure, although not completely stationary, maintains a distinct morphology. (*b*) Horizontal samples of the average scan at altitudes from 200 to 400 km. These samples have been shifted so that magnetic field lines are vertical in order to emphasize the field alignment of the cavity. This stack plot shows that the cavity is most easily identified at altitudes from 250 to 325 km and is clearly field-aligned.

same drift context described by *Weber et al.* [1991] for a midnight sector arc. Although the velocity shear may be related to a system of field-aligned currents associated with the arc, essentially coupling the local arc drift with local arc electrodynamics, there is no evidence that the arc/cavity pair is oriented parallel to the large-scale flow direction. The drift process of cavity formation is therefore considered unlikely for this event. In order for the FAC process to work, a sufficiently large amount of the downward "evacuation" current must close in the ionosphere. The divergence of this closure current must equal the observed thermal electron loss rate as measured by the radar. Although this experiment provided accurate measurements of off-meridional ion velocity (and thus electric fields), suggesting that a system of radar-derived FACs can ultimately be determined, this detailed calculation was not performed herein. An estimate of the downward FAC associated with the cavity, based on the observed velocity shear and derived conductivity structure, however, yields a value of 0.24 μA m^{-2}, which is consistent with the magnitude of cavity-related downward FACs reported in paper 1. This experiment additionally underscored the *Doe et al.* [1993] observation of cavities adjacent to height-integrated conductivity gradients on the order of 100 μmhos m^{-1} that were found to be sufficient to support the FAC mechanism.

The cavity shown in Plate 2, while narrower than previous observations, is not short-lived or obscured

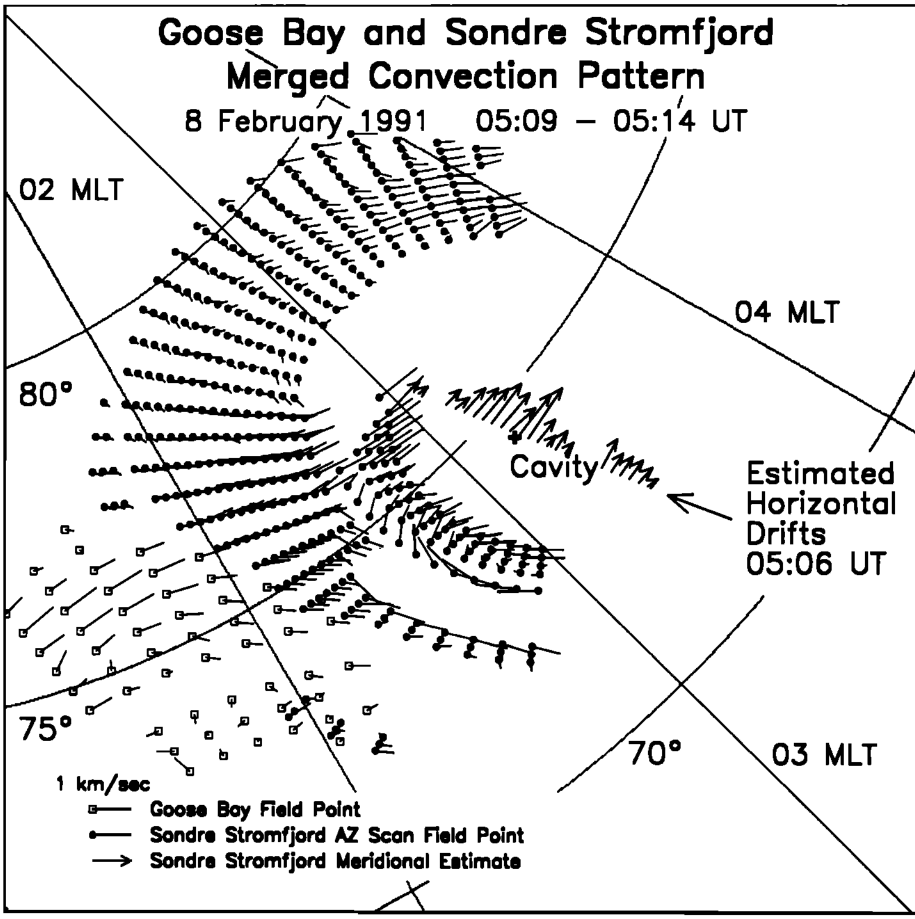

Fig. 8. A composite of Sondrestrom meridional estimates at 0506 UT with merged velocities from overlapping Sondrestrom/Goose Bay scans measured from 0509 to 0514 UT. Line-of-sight vector components from Goose Bay and Sondrestrom data were filtered to remove measurements with absolute errors larger than 200 m s^{-1}, smoothed by a 1 km s^{-1} median filter across azimuth and range and projected into PACE geomagnetic coordinates at 350 km. Line-of-sight components were then merged for collocated scatter volumes to form a set of seed vectors used to modify remaining line-of-sight vectors under a divergence-free flow assumption. The composite convection pattern shows that estimated eastward drifts at 0506 UT, and at later times, are part of a much larger W-E flow channel which extends over almost 3 hours of MLT.

by drifting enhancements. All available drift data suggest strong cross-arc drift during the period of cavity formation, casting doubt on the drift mechanism. The close proximity of a significant conductivity gradient to the cavity can alternatively be interpreted in the framework of a current system. In such a scenario, the narrow field-aligned finger of ionization associated with the cavity would be caused by an upward field-aligned current, presumably associated with relatively soft, quiet time precipitation. This current would close to an evacuation current over the cavity. This cavity event is therefore attributed to a field-aligned current poleward of the traditional region 1 current system, perhaps similar to the IMF B_z north system recently suggested by *Taguchi* [1992].

The radar observations of February 8, 1991, with a stationary arc assumption, show that the cavity and associated arc remain as a streamline-oriented pair for a 30-min period. Steady field-aligned currents, drifts or a combination of the two mechanisms could explain this observation.

6. CONCLUSIONS

This study considered convective distortion and field-aligned evacuation mechanisms as the primary processes for the creation of auroral cavities. Although paper 1 concluded that localized field-aligned currents were the most probable cause of cavities, the convection mechanism could not be completely ruled out without additional drift observations and modeling. The model presented in section 2 suggests that the drift process can be confirmed by observing the orientation of an elongated cavity parallel to a local convection streamline, provided events are studied that are far from regions of significant flow divergence.

The convective distortion model additionally suggests that a typical drift pattern can transform a density depression on the scale of a typical polar hole into an auroral cavity over a time scale short enough for the convection pattern to remain stable (~3 hours). The resultant cavity should be azimuthally elongated and relatively long-lived. The initial location of the required seed in the morning sector, however, is not corroborated by either polar hole satellite measurements (*Brinton et al.* [1978]; *Benson and Calvert* [1979]; *Persoon et al.* [1988]; *Hoegy and Grebowsky* [1991]) or modeling studies [*Sojka et al.* 1981].

The February 1991, cavity detection campaign, designed to differentiate between drift and FAC processes, was not able to decide definitively between the two mechanisms. In the cases considered, convincing evidence for the drifting gradient mechanism could not be found. The lack of consistent observations for cavities elongated by more than 16 min MLT (120 km), or for cavities oriented along the large-scale flow direction, suggest that a more local causal mechanism is required. The observation that cavities are always collocated with auroral arcs, most of which have arc-related shears, thus offers indirect support for the downward field-aligned current mechanism. Clearly, additional observations and modeling work is required. A fluid simulation of plasma evacuation by the closure of field-aligned currents will be presented in a subsequent paper.

Acknowledgments. The IS radar data were gathered through the efforts of the SRI Sondrestrom Incoherent Scatter Radar Facility site crew. Operations were approved through the Danish Commission for Scientific Research in Greenland. Organized logistical planning and post-experiment IS radar processing would have been impossible without the help of M. McCready. Special thanks go to C. J. Heinselman for helping define the off-meridional antenna pointing positions and R. C. Livingston for helping process the resulting ionospheric data. J. Baumgardner, G. Ruiz-Camauer, and H. Pais are recognized for their work in the design, fabrication, integration and ongoing evolution of the CEDAR all-sky imaging system. D. Nottingham is acknowledged for operating the all-sky imager and for writing the image analysis software. The authors also thank R. P. Lepping for providing IMP 8 magnetometer data and E. Weber for providing prepublication results during the refereeing process. R. Robinson provided helpful comments during the refereeing period. This study was supported at Boston University by National Science Foundation (NSF) grants ATM-9102557 and ATM-9012786. Work at SRI was supported by the NSF under cooperative agreement ATM-8822560 and at the Johns Hopkins University Applied Physics Laboratory by NSF grant ATM-903860 and National Aeronautics and Space Administration (NASA) grant NAGS-1099.

REFERENCES

Anderson, D. N., J. Buchau, and R. A. Heelis, Origin of density enhancements in the winter polar cap, *Radio Sci., 23,* 513, 1988.

Baker, K. B., and S. Wing, A new magnetic coordinate system for conjugate studies at high latitudes, *J. Geophys. Res., 94,* 9139, 1989.

Benson, R. F., and W. Calvert, ISIS 1 observations at the source of auroral kilometric radiation, *Geophys. Res. Lett., 6,* 479, 1979.

Block, L. P., and C.-G. Fälthammar, Effects of field aligned currents on the structure of the ionosphere, *J. Geophys. Res., 73,* 4807, 1968.

Brinton, H. C., J. M. Grebowsky, and L. H. Brace, The high latitude winter *F* region at 300 km: Thermal plasma observations from AE-C, *J. Geophys. Res., 83,* 4767, 1978.

de la Beaujardiere, O., R. Vondrak, and M. Baron, Radar observations of electric fields and currents associated with auroral arcs, *J. Geophys. Res., 82,* 5051, 1977.

Doe, R.A., M. Mendillo, J. Baumgardner, J. Vickrey, and R. Eastes, Coordinated imaging and radar studies of ionospheric cavities at auroral latitudes (abstract), *Eos Trans. AGU, 70,* 416, 1989.

Doe, R.A., M. Mendillo, J. Vickrey, L. Zanetti and R. Eastes, Observations of nightside auroral cavities, *J. Geophys. Res., 98,* 293, 1993.

Feldstein, Y. I., and G. V. Starkov, Dynamics of auroral belt and polar geomagnetic disturbances, *Planet. Space Sci., 15,* 209-229, 1967.

Gallagher, H. A., E. J. Weber, J. F. Vickrey, and R. L. Carovillano, Plasma flows associated with an auroral arc at the polar cap boundary, in *Auroral Plasma Dynamics, Geophys. Monogr. Ser.*, edited by R. L. Lysak, vol. 80, pp. 81-88, AGU, Washington, D. C., 1993.

Heelis, R. A., J. K. Lowell, and R. W. Spiro, High latitude ionospheric convection model, *J. Geophys. Res., 87,* 6339, 1982.

Heelis, R. A., and J. F. Vickrey, Magnetic field-aligned effects on ionospheric plasma structure, *J. Geophys. Res., 95,* 7995, 1990.

Heelis, R. A., Modeling ion concentration patches in the high-latitude ionosphere, paper presented at the Joint High-Latitude Plasma Structure and Global Aspects of Plasma Structure (HLPS/GAPS) Workshop, Peaceful Valley, Colo., National Science Foundation, Washington, D. C., June 18-20, 1992.

Heppner, J. P., and N. C. Maynard, Empirical high-latitude electric field models, *J. Geophys. Res., 92,* 4467, 1987.

Hoegy, W. R., and J. M. Grebowsky, Dependence of polar hole density on magnetic and solar conditions, *J. Geophys. Res., 96,* 5737, 1991.

Holt, J. M., R. H. Wand, J. V. Evans, and W. L. Oliver, Empirical models for plasma convection at high latitudes from Millstone Hill observations, *J. Geophys. Res., 92,* 203, 1987.

Kelley, M. C., *The Earth's Ionosphere,* p. 350, Academic, San Diego, Calif., 1989.

Klumpar, D. M., Relationships between auroral particle distributions and magnetic field perturbations with field-aligned currents, *J. Geophys. Res., 84,* 6524, 1979.

Persoon, A. M., D. A. Gurnett, W. K. Peterson, J. H. Waite, Jr., J. L. Burch, and J. L. Green, Electron density depletions in the nightside auroral zone, *J. Geophys. Res., 93,* 1871, 1988.

Rich, F. J., W. J. Burke, M. C. Kelley, and M. Smiddy, Observations of field-aligned currents in association with strong convection electric fields at subauroral latitudes, *J. Geophys. Res., 85,* 2335, 1980

Robinson, R. M., R. T. Tsunoda, J. F. Vickrey, and L. Guerin, Sources of *F* region ionization enhancements in the nighttime auroral zone, *J. Geophys. Res., 90,* 7533, 1985.

Ruohoniemi, J. M., R. A. Greenwald, K. B. Baker, J.-P. Villain, and M. A. McCready, Drift motions of small-scale irregularities in the high latitude *F* region: An experimental comparison with plasma drift motions, *J. Geophys. Res., 92,* 4553, 1987.

Ruohoniemi, J. M., R. A. Greenwald, K. B. Baker, J.-P. Villain, C. Hanuise, and J. Kelly, Mapping high-latitude convection with coherent HF radars, *J. Geophys. Res., 94,* 13,463, 1989.

Sojka, J. J., W. J. Raitt, and R. W. Schunk, A theoretical study of the high-latitude winter *F* region at solar minimum for low magnetic activity, *J. Geophys. Res., 86,* 609, 1981.

Solomon, S. C., P. B. Hays, and V. J. Abreu, The auroral 6300-Å emission: Observations and modeling, *J. Geophys. Res., 93,* 9867, 1988.

Taguchi, S., B_y-Controlled field-aligned currents near the midnight auroral oval during northward interplanetary magnetic field, *J. Geophys. Res., 97,* 12,231, 1992.

Weber, E. J., J. F. Vickrey, H. Gallagher, L. Weiss, C. J. Heinselman, R. A. Heelis, and M. C. Kelley, Coordinated radar and optical measurements of stable auroral arcs at the polar cap boundary, *J. Geophys. Res., 96,* 17,847, 1991.

(Received December 1, 1992; revised July 15, 1993; accepted July 16, 1993.)